ACS Biomaterials SCIENCE & ENGINEERING

Letter

pubs.acs.org/journal/abseba

Elastoplastic Deformation of Silk Micro- and Nanostructures

Guoyou Huang,[†,‡,§] Limei Tian,[†] Keng-Ku Liu,[†] Bo Hu,[†] Feng Xu,[‡,§] Tian Jian Lu,[‡,§] Rajesh R. Naik,[∥] and Srikanth Singamaneni*[,†]

[†]Department of Mechanical Engineering and Materials Science and Institute of Materials Science and Engineering, Washington University in St. Louis, St. Louis, Missouri 63130, United States

[‡]MOE Key Laboratory of Biomedical Information Engineering, School of Life Science and Technology, and [§]Bioinspired Engineering and Biomechanics Center (BEBC), Xi'an Jiaotong University, Xi'an 710049, P.R. China

[∥]Soft Matter Materials Branch, Materials and Manufacturing Directorate, and 711 Human Performance Wing, Wright-Patterson Air Force Base, Dayton, Ohio 45433, United States

Supporting Information

ABSTRACT: Excellent mechanical strength, programmable biodegradation, optical transparency, and extremely low surface roughness of reconstituted silk micro- and nanostructures makes them highly attractive for a broad range of applications in biophotonics, bioresorbable electronics, and targeted drug delivery. The mechanical behavior of reconstituted silk structures at micro- and nanometer length scales is not well understood because of the challenges associated with testing of silk structures at these length scales. In this study, we demonstrate the fabrication of low-dimensional patterned silk films and silk micro- and nanopillars and their transfer to stretchable substrates. The silk micro- and nanostructures exhibited extremely high ductility with large local deformation (up to ~230% local strain) and the extent of local deformation before failure was found to be secondary structure-dependent. The successful transfer of the patterned silk films to stretchable substrates without the use of any organic solvent enabled us to probe the changes in the secondary structure of silk micro- and nanostructures upon mechanical deformation. Our results provide novel insight into the structure−function relationship of silk materials, and hold promise for applications in tissue engineering, controlled drug delivery, and electronic and optical devices.

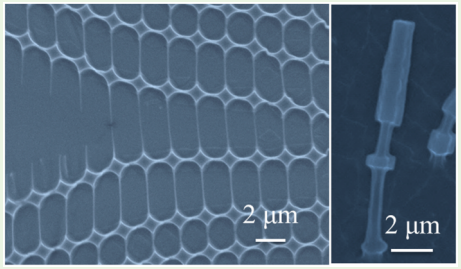

KEYWORDS: *silk, micro- and nanostructures, template-assisted, secondary structure, micro-Raman spectroscopy*

Through the process of natural selection, biological systems have successfully developed a rich variety of structural and functional materials that exhibit unique mechanical, optical, magnetic, catalytic, and thermal properties.[1−4] Because of their unique physical, chemical, and biological properties, materials based on natural proteins have attracted significant interest for a wide variety of applications.[5−7] One such abundantly available protein polymer is silk fibroin from *Bombyx mori* silkworm cocoon, which has been reconstituted and engineered into different material forms including fibers, tubes, films, particles, sponges, and gels.[8] Silk materials have found broad applications in tissue engineering, drug delivery, electronic, and optical devices.[6,9−11] The excellent processing ability of silk fibroin has enabled the fabrication of micro- and nanostructures with high fidelity to the micro- and nanotemplates.[12]

Silk fibers are among the strongest natural polymeric materials with a unique combination of high modulus and high elongation at failure.[13,14] The multidomain structure of the silk fibroin heavy chain plays a key role in increasing the toughness of silk fibers to record values. In native silk from silkworm, *Bombyx mori*, the presence of GAGAGS, GAGAGY, GAGAGA, and GAGYGA repeats results in the formation of β-sheet crystallites, which are dispersed in less-ordered semi-amorphous matrix. Because of such natural domain/composite structure, silk materials possess outstanding mechanical properties, particularly high tensile strength (0.5−3 GPa).[15,16] While native silk fibers are known to exhibit a combination of high modulus and high elongation to failure (leading to high toughness), reconstituted silks are rather brittle. It has been recognized that the mechanical properties of silk materials strongly depend on their secondary structure.[17,18] Silk fibroin in freshly prepared aqueous solution typically exhibits amorphous random coil secondary structure and forms silk I, characterized by crank-shaft conformation. Both amorphous silk and silk I are water-soluble. However, when subjected to organic solvent treatment such as methanol, water vapor, heat and/or mechanical strain, they can crystallize and convert to extremely stable and water insoluble silk II.[19,20] Silk II is characterized by beta pleated sheet structure stabilized by interchain hydrogen bonding, showing enhanced elastic modulus and mechanical strength compared to silk I. The relative content and distribution of silk II in silk materials play critical roles in their biodegradability, dielectric, and mechanical properties.[21,22] In addition, as demonstrated in other polymeric materials,[23]

Received: April 1, 2016
Accepted: May 8, 2016

DOI: 10.1021/acsbiomaterials.6b00177
ACS Biomater. Sci. Eng. XXXX, XXX, XXX−XXX

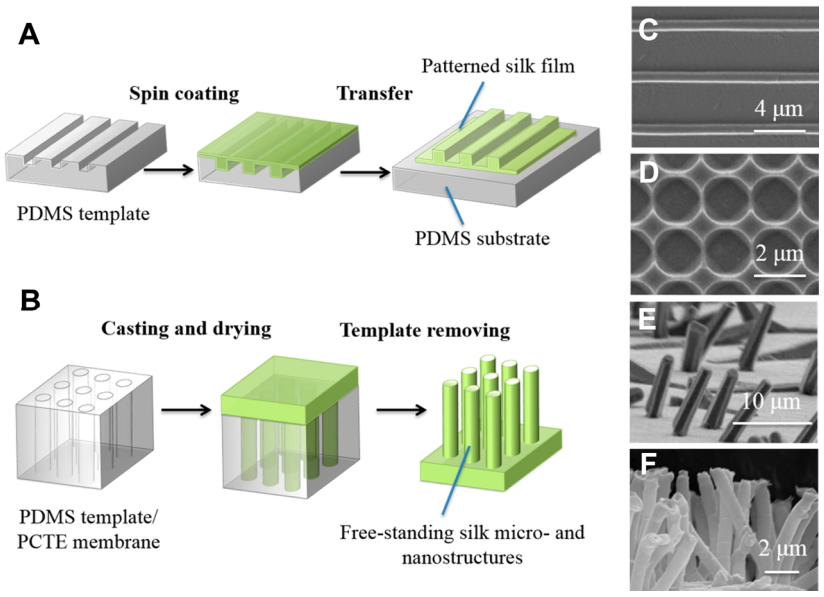

Figure 1. (A) Schematic illustration showing the fabrication of silk thin films. Silk fibroin solution was first spin coated and dried on PDMS template to form patterned silk films, which were then transferred to soft and tacky PDMS substrates. (B) Schematic illustration showing the fabrication of silk micro- and nanopillars. Silk fibroin solution was cast and dried on PDMS template with microholes or polycarbonate track etch membrane, which were peeled off to result in free-standing silk micro- and nanopillars. Representative SEM images of (C) stripe patterned silk film, (D) grid patterned silk film, (E) free-standing silk micropillars and (F) free-standing silk nanotubes.

dimensional and scale effects may also significantly affect the mechanical performance of silk materials.[15,24]

The mechanical behavior of reconstituted silk at micro- and nanometer length scales and the associated conformational changes have not been investigated. We therefore developed methods to fabricate low-dimensional silk micro- and nanostructures in native silk I state, and investigated their deformation and resultant secondary structure changes under external mechanical stress. Significantly, the silk micro- and nanostructures exhibited extremely high (up to 230%) local deformations, reminiscent of elastoplastic deformation. The degree of deformation was found to be highly dependent on the conformation of silk micro- and nanostructures. Changes in the secondary structure of silk micro- and nanostructures exhibiting large elastoplastic deformation were probed using micro-Raman spectroscopy.

To fabricate silk micro- and nanostructures, researchers have employed various methods including spin-coating and soft lithography.[24−28] The mechanical properties of ultrathin (<100 nm) supported or free-standing silk films obtained by spin-coating or spin-assisted layer-by-layer (LbL) assembly have been studied using a variety of methods, such as buckling, bulging, and surface force spectroscopy.[15] The ultrathin films are often released from solid substrates and transferred to soft substrates such as poly(dimethylsiloxane) (PDMS) or freely suspended over holey substrates for compressive or tensile testing. Soft lithography has been extensively employed to fabricate silk films with custom-designed patterns such as silk microprism array for optical applications.[29] Here, we employ soft lithographic techniques to fabricate low-dimensional silk films with predefined surface patterns. These patterned silk films were then transferred to soft PDMS substrates with and without methanol treatment. The ability to transfer silk films onto these substrates without using any organic solvent enabled us to investigate the elastoplastic deformation of ultrathin films in silk I state. Moreover, the surface patterns on silk films served as micro/nanoscale markers, enabling quantification of local deformation of silk films under uniaxial stretching. Upon external tensile stress, the ultrathin silk films and one-dimensional (1D) nanostructures exhibited large elastoplastic deformation. Confocal Raman microscopy revealed concomitant secondary structure changes in highly deformed regions (i.e., strain induced conformation transition). The extent of elastoplastic deformation of silk micro- and nanostructures was found to be highly dependent on the secondary structure of silk.

The methods for fabricating surface-patterned silk films and free-standing silk micro- and nanopillars are illustrated in Figure 1A, B, respectively. PDMS templates with different negative patterns were obtained by curing PDMS prepolymer and cross-linking agent at a mass ratio of 8:1 at 80 °C for 3 h (Figures S1A, B and S2A, C). Subsequently, 10 μL of silk fibroin solution at a concentration of 5% (m/v) was added to cover the negative patterns on PDMS template, followed by spin coating at a speed of 3000 rpm for 30 s. The patterned silk films were then transferred to soft PDMS substrates before or after methanol treatment for further studies. The soft PDMS substrates prepared by curing PDMS prepolymer and cross-linking agent at a mass ratio of 20:1 at 70 °C for 1 h showed much stronger adhesion with silk films compared to PDMS templates, and thus can easily peel off silk films without the use of any organic solvent. SEM imaging revealed silk films with micro/nanopatterns replicated with high fidelity (Figure 1C, D and Figure S2B, D and Table S1). For example, the width of the silk stripes (~760 nm) in the stripe patterned silk film is remarkably close to that of the grooves in the corresponding PDMS template.

Silk micro- and nanopillars were fabricated using two different templates (Figure S1C, D). Silk micropillars were obtained using PDMS templates with microholes molded from grown ZnO microwires on silicon substrate.[30] Silk fibroin solution was casted and dried on the PDMS template at room

DOI: 10.1021/acsbiomaterials.6b00177
ACS Biomater. Sci. Eng. XXXX, XXX, XXX−XXX

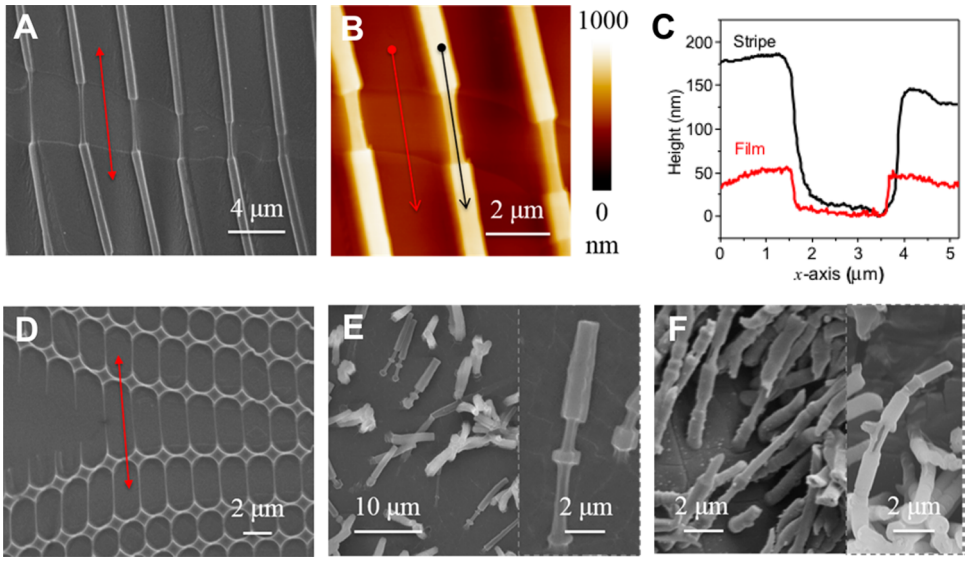

Figure 2. (A) SEM image of stretched silk film with stripe pattern. (B) AFM height image of stretched stripe patterned silk film. (C) Height profile along the indicated arrows in B. SEM image of (D) stretched grid patterned silk film, (E) deformed silk micropillars, and (F) deformed silk nanotubes.

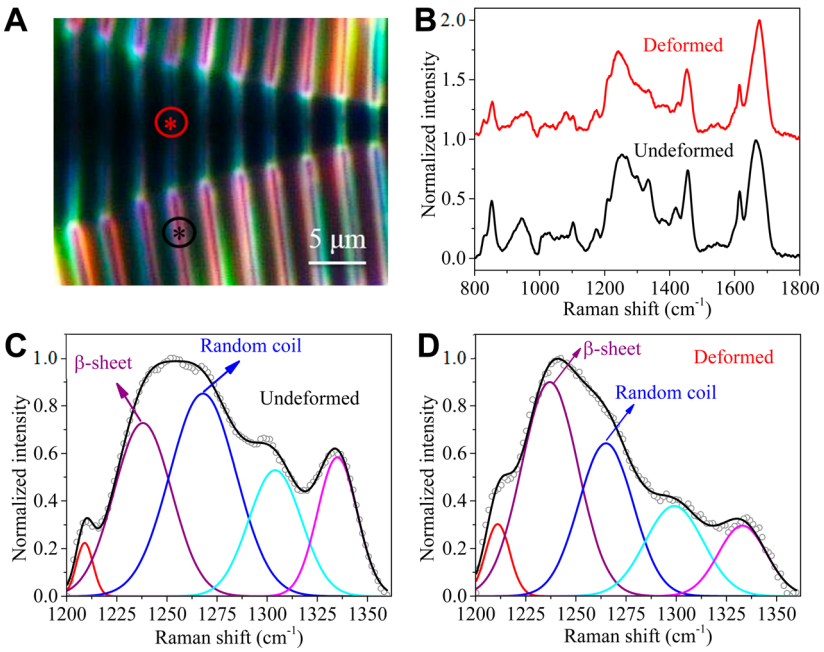

Figure 3. (A) Dark-field image of stretched stripe-patterned silk film. The star symbols indicate the regions where Raman spectra were collected. (B) Raman spectra of silk stripes from undeformed (black) and necked (red) regions. Zoom-in of the amide III Raman band from (C) undeformed and (D) necked regions with deconvoluted peaks.

temperature, and manually peeled off with tweezers to obtain free-standing silk micropillars (Figure 1E). To fabricate free-standing silk nanotubes, we employed polycarbonate track-etched (PCTE) membrane with 800 nm diameter pores as template. Silk hollow nanopillars (i.e., silk nanotubes) were fabricated by applying a wetting template method,[31] in which the wall thickness of the hollow nanopillars can be easily controlled by adjusting the concentration of silk fibroin solution (Figure 1F).

To investigate the mechanical behavior of patterned silk films, we stretched soft PDMS substrates uniaxially to induce deformation in the silk film. The stripes on silk films clearly showed necking-like behavior under stretching (Figure 2A). Although necking was also observed in the continuous silk film below the stripes (surface relief structures), the silk stripes made the neck-like local deformation clearly visible (Figure 2B, C). Local extension ratio was calculated from the stretched grid patterned silk films, which revealed a local ultimate strain of 230% (Figure 2D). The ductile or elastoplastic behavior of patterned silk films was further studied in silk micro- and nanopillars by stretching 1D micro- and nanostructures using solid adhesive by gentle contact followed by slow peeling. This tape peeling test results in a complex interplay of forces, revealing the mechanical response of silk structures in a wide variety of deformational modes. While the initial contact with the adhesive tape results in axial and radial compression of the

DOI: 10.1021/acsbiomaterials.6b00177
ACS Biomater. Sci. Eng. XXXX, XXX, XXX−XXX

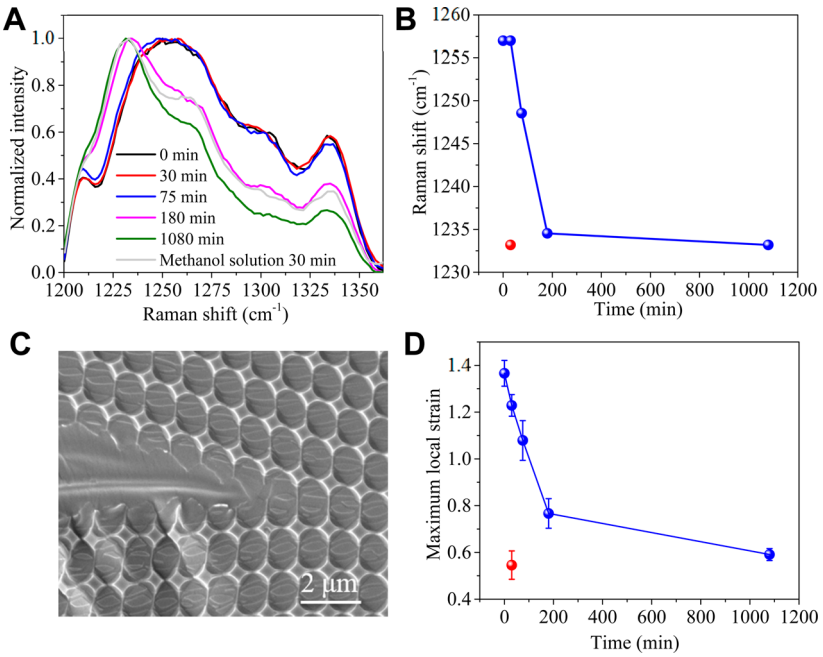

Figure 4. (A) Raman spectra of grid patterned silk films treated with methanol vapor for different durations. The Raman spectra of grid patterned silk film treated with methanol solution for 30 min is included. (B) Plot of the dominant Raman band position in amide III region as a function of methanol vapor treatment time. The corresponding band position of grid patterned silk film treated with methanol solution for 30 min is included (red symbol). (C) SEM image of stretched grid patterned silk treated with methanol vapor for 18 h. (D) Local ultimate strain of the grid patterned silk films treated with methanol vapor for different durations. The local ultimate strain in grid patterned silk film treated with methanol solution for 30 min is included (red symbol). Error bars in D are standard deviation with $n \geq 5$.

micro- and nanostructures, the peel off process results in a complex tensile and shear deformation in the 1D nanostructures. High ductility was observed for both silk micropillars and hollow nanopillars as shown separately in Figure 2E, F. Such high ductility has never been reported for dried silk materials. Polymeric materials are known to exhibit length scale-dependent mechanical behavior such as large ductility in low-dimensional structures.[23] Similar phenomenon might be at play for silk micro- and nanostructures studied here. The possible reason for such length-scale dependent mechanical properties is the enhanced polymer chain mobility at the surface due to the significantly lower entanglement density at the surface compared to the bulk. However, a more detailed study focused on the thermomechanical properties (e.g., depression in glass transition temperature) of silk films with different thickness can provide more insight into the mechanistic aspects of the length scale-dependent mechanical behavior.

Stripe patterned silk films were further investigated to study the effects of mechanical deformation on secondary structure changes in silk films (Figure 3). Different methods including Fourier transform infrared spectroscopy (FTIR),[21] nuclear magnetic resonance (NMR),[32] X-ray diffraction (XRD),[33] and circular dichroism,[34] have been explored to probe the conformational changes of silk materials. These methods either require a large quantity of samples or do not provide sufficient spatial resolution to probe the local secondary structure of deformed micro- and nanostructures. Owing to its rich conformational specificity and excellent spatial resolution, we employed micro-Raman spectroscopy to monitor the changes in the secondary structure of silk.[35] Noting that Raman bands of PDMS partially overlap with those of silk, silk films having surface patterns were transferred to micropatterned soft PDMS substrates. Taking advantage of the confocality of the micro-Raman system employed in our study and acquiring the Raman spectra from receding portions of micropatterned PDMS (i.e., from freely suspended regions), we managed to greatly reduce the background signals from PDMS substrate. We investigated deformation-induced changes in the secondary structure of silk by obtaining Raman spectra from deformed (i.e., necked) and undeformed regions of stripe patterns (Figure 3A). Raman spectra in the range of 800−1800 cm^{-1} from both deformed and undeformed regions exhibited characteristic bands corresponding to silk protein (Figure 3B).[35,36] The assignment of the major bands observed in the spectra is provided in the Table S2. The Raman spectra showed intense bands in conformation-sensitive amide I (1660 cm^{-1}) and amide III regions (~1230−1275 cm^{-1}). The amide III region comprises a number of bands including the dominant C−N−H in-plane bending and C−N stretching modes, and is known to be sensitive to changes in silk secondary structure.[12,37]

To uncover secondary structure changes in deformed silk stripes, we deconvoluted the Raman spectrum in amide III region of Figure 3B into five Gaussian peaks (Figure 3C,D). In the undeformed regions, the most intense band was found to be at 1264 cm^{-1}, which corresponds to random coil and α-helical secondary structures of silk chains (Figure 3C). On the other hand, in the necked regions, the most intense peak occurred at 1231 cm^{-1}, indicative of antiparallel β-sheet structures (Figure 3D). Furthermore, the amide I peak at 1660 cm^{-1}, corresponding to C═O stretching, was found to be sharper.[12] Although the spin-coating process may induce a change in the secondary structure silk (from silk I to silk II), this transition is confined to the thin interfacial regions (<5 nm at substrate−film interface).[15] Such transition from silk I to silk II has been successfully employed to fabricate silk-on-silk ultrathin films, microcapsules and interfacial coatings using spin-assisted layer-

DOI: 10.1021/acsbiomaterials.6b00177
ACS Biomater. Sci. Eng. XXXX, XXX, XXX−XXX

by-layer assembly.[15] Beyond the substrate−film interfacial region, the spin-coated film exhibits primarily silk I structure as evidenced by the Raman spectra of undeformed stripe segments, which are rich in random coil and α-helical secondary structures (Figure 3C). However, Figure 3D showed that the locally necked stripe segments were dominated by silk II, suggesting that the transition of silk secondary structures from silk I to silk II occurred indeed during stretching.

Strain-induced molecular chain orientation[38] and conformation[37] changes have been reported by stretching bulk regenerated silk films and concentrated silk dope solution, respectively. However, our work demonstrates a strain-induced conformation change in dried reconstituted silk fibroin, ruling out the contribution of dehydration on conformation transition during stretching. Moreover, it is also the first demonstration of strain-induced conformation transition of reconstituted silk fibroin at the microscale, confirmed using micro-Raman spectroscopy. To further understand the relationship between elastoplastic deformation of reconstituted silk fibroin and their secondary structures, we uniaxially stretched grid patterned silk films treated with methanol vapor for different durations. The down shift of Raman band from 1260 to 1230 cm^{-1} unambiguously indicated the transformation from silk I to silk II (Figure 4A). The extent of such transition depended upon the duration of methanol vapor treatment, with most of the transition occurring between 75−180 min (Figure 4B). Stretching tests showed that the ductility of grid patterned silk films decreased after methanol treatment (Figure 4C and Figure S3). The local ultimate strain of the ligaments decreased to 45% for films treated with methanol vapor for 3 h (Figure 4D). Although this ultimate strain is significantly lower compared to that observed in untreated films (exhibiting ∼230% local strain), it is still significantly higher than those of most bulk fibrous materials.[15,39] The reduction in the ductility of silk films is consistent with the increase in the β-sheet content of silk films, revealing the important role of secondary structures on silk elastoplastic deformation (Figure 4B, D). It has been reported that the elastic modulus of silk materials increases with increasing silk II content.[6] Our results indicate that the transition from silk I to silk II state, which may result in an increase in elastic modulus, is accompanied by decreasing (local) ductility. The limitations of current study include: First, we are not able to quantify the mechanical load applied to silk micro- and nanostructures (e.g., silk micropillars), so the study does not provide insight into quantitative stress−strain behavior of the micro- and nanostructures. Second, advanced measurements such as nano-IR may provide additional insight into the changes in the secondary structure of silk micro- and nanostructures upon deformation.

In summary, we have demonstrated facile methods to fabricate low-dimensional patterned silk films and silk micro- and nanopillars. The successful transfer of the patterned silk films to stretchable substrates without using any organic solvent enabled us to investigate the relationship between their secondary structures and mechanical properties starting with native conformation. These low-dimensional silk materials showed extremely high local ductility that critically depended on the secondary structures. Strain induced conformation transition was observed in dry reconstituted silk materials at the micro and nanoscale. These results may provide insights into structure−function relationship of silk materials at micro and nanoscale, and hold promise for applications in tissue engineering, controlled drug delivery and release, and electronic and optical devices. The elastoplastic deformation and length-scale dependent mechanical properties of silk fibroin can be harnessed to overcome the brittle nature of reconstituted silk structures through careful design of the load bearing elements.

EXPERIMENTAL SECTION

Fabrication of Silk Micro- and Nanostructrues. PDMS templates with relief patterns were prepared by curing PDMS prepolymer and cross-linking agent (Dow Corning Sylgard 184 Silicone Elastomer Kit) at a mass ratio of 8:1 at 80 °C for 3 h on microfabricated silicon masters. PDMS template with microholes for fabricating silk micropillars was molded from grown ZnO microwires on silicon substrate using Au as a seed layer.[30] PCTE membrane with average pore diameter of 800 nm (Sterlitech, Inc.) was used for fabricating silk nanotubes. Silk fibroin was reconstituted from *Bombyx mori* silkworm cocoon according to a reported protocol.[8] The degumming time was controlled to be 30 min. The final concentration of silk fibroin was measured to be 5% (w/v). To fabricate patterned silk films, we added 10 μL of silk fibroin solution onto the surface of PDMS templates and spun (model WS-400, Laurell Technologies Corporation) at 3000 rpm for 30 s. A tacky PDMS substrate was then gently attached to the silk covered PDMS template and then separated to transfer the patterned silk films. To obtain grid patterned silk films with different contents of secondary structures, silk films were treated with saturated methanol vapor for 30, 75, 180, and 1080 min, before transferring them to tacky PDMS substrates. To prepare silk micro- and nanopillars, 10 μL of silk fibroin solution was cast onto PDMS template with microholes or PCTE membrane and dried at room temperature for 3 h. Silk film with micropillars was separated from the PDMS templates using tweezers. PCTE membrane was removed by dissolving the membrane with dichloromethane (Sigma-Aldrich).

Mechanical Testing and Characterization of Silk Micro- and Nanostructures. Stretching of surface patterned silk films was achieved by manually stretching the soft PDMS substrate. The stretched samples were held on a small piece of glass slide (∼1 × 2 cm) with adhesive tape for further characterization. Silk micro- and nanopillars were deformed by applying an adhesive tape to adhere and stretch their free ends by peeling. Scanning electron microscope (SEM) images were obtained using a FEI Nova 2300 field emission SEM at an acceleration voltage of 10 kV. The samples were sputter coated with a 4−8 nm thick Au layer before SEM imaging. ImageJ (Version 1.48) was used to analyze the SEM images. The local ultimate strain of the stretched grid patterned silk films was calculated as $\varepsilon = (L_1 + L_2 - L_0)/L_0 \times 100\%$. L_0, L_1, and L_2 indicate the length of the corresponding deformed structures as indicated in Figure S4. Atomic force microscopy (AFM, Bruker Dimension 3000) was used to image deformed stripe patterned silk film in light tapping mode. Triangular Si cantilevers with tip radius less than 10 nm (MikroMasch) were employed for AFM imaging. WSxM software (version 3.1) was used to measure thickness changes of silk stripes and silk films at the necked regions.

Raman Spectroscopy Characterization of the Secondary Structures. To obtain Raman spectra of silk and reduce the background signal of PDMS substrate, patterned silk films were transferred to soft PDMS substrate with ∼50 μm diameter ×50 μm height holding holes on the surface. Raman spectra of the suspended silk patterns above the holes were obtained with Renishaw inVia confocal Raman Spectrometer mounted on a Leica microscope (Leica DM LM) with 100× objective (NA = 0.85) at an excitation wavelength of 514 nm (Ar laser). Each spectrum was obtained with one accumulation and 60 s exposure time. At least 5 spectra for each sample were collected and averaged to increase signal-to-noise ratio. To subtract the PDMS background, the Raman spectra of silk and PDMS were obtained and it was found that PDMS has an intense characteristic band around 771 cm^{-1}, whereas silk does not show any Raman band at that frequency, see Figure S5A (the intense peak around 970 cm^{-1} corresponds to silicon substrate). So 771 cm^{-1} was used as the reference peak. Both Raman spectra of PDMS well (I) and silk patterns suspended over the PDMS well (I') were normalized

DOI: 10.1021/acsbiomaterials.6b00177
ACS Biomater. Sci. Eng. XXXX, XXX, XXX−XXX

corresponding to the intensity at 771 cm^{-1}, Figure S5B. The PDMS background was subtracted by performing $I'/I'_{771} - I/I_{771}$, Figure S5C. Identical procedure was employed for spectra obtained before and after deformation of the silk patterns. Gaussian function was used for peak deconvolution, which was performed in OriginPro 8.6 (OriginLab Corp.).

■ ASSOCIATED CONTENT

Supporting Information

The Supporting Information is available free of charge on the ACS Publications website at DOI: 10.1021/acsbiomaterials.6b00177.

Figures S1−S5 and Tables S1 and S2 (PDF)

■ AUTHOR INFORMATION

Corresponding Author

*E-mail: singamaneni@wustl.edu.

Notes

The authors declare no competing financial interest.

■ ACKNOWLEDGMENTS

We acknowledge support from Air Force Office of Scientific Research (S.S., Award FA9550-15-1-0228; and R.R.N., 12RX11COR) and AFRL/RX. This work was supported by the International Science and Technology Cooperation Program of China (2013DFG02930) and the China Postdoctoral Science Foundation (2013M540742). The authors thank the Nano Research Facility (NRF) at Washington University for providing access to electron microscopy facilities.

■ REFERENCES

(1) Wegst, U. G. K.; Bai, H.; Saiz, E.; Tomsia, A. P.; Ritchie, R. O. Bioinspired structural materials. *Nat. Mater.* **2015**, *14* (1), 23−36.

(2) Naleway, S. E.; Porter, M. M.; McKittrick, J.; Meyers, M. A. Structural design elements in biological materials: application to bioinspiration. *Adv. Mater.* **2015**, *27* (37), 5455−5476.

(3) Zhao, N.; Wang, Z.; Cai, C.; Shen, H.; Liang, F.; Wang, D.; Wang, C.; Zhu, T.; Guo, J.; Wang, Y.; Liu, X.; Duan, C.; Wang, H.; Mao, Y.; Jia, X.; Dong, H.; Zhang, X.; Xu, J. Bioinspired materials: from low to high dimensional structure. *Adv. Mater.* **2014**, *26* (41), 6994−7017.

(4) Vollrath; Fritz; Knight; David, P. Liquid crystalline spinning of spider silk. *Nature* **2001**, *410* (6828), 541−548.

(5) Gillette, B. M.; Jensen, J. A.; Tang, B. X.; Yang, G. J.; Bazargan-Lari, A.; Zhong, M.; Sia, S. K. In situ collagen assembly for integrating microfabricated three-dimensional cell-seeded matrices. *Nat. Mater.* **2008**, *7* (8), 636−640.

(6) Kundu, B.; Kurland, N. E.; Bano, S.; Patra, C.; Engel, F. B.; Yadavalli, V. K.; Kundu, S. C. Silk proteins for biomedical applications: Bioengineering perspectives. *Prog. Polym. Sci.* **2014**, *39* (2), 251−267.

(7) Porter, D.; Vollrath, F. Silk as a biomimetic ideal for structural polymers. *Adv. Mater.* **2009**, *21* (4), 487−492.

(8) Rockwood, D. N.; Preda, R. C.; Yucel, T.; Wang, X.; Lovett, M. L.; Kaplan, D. L. Materials fabrication from Bombyx mori silk fibroin. *Nat. Protoc.* **2011**, *6* (10), 1612−1631.

(9) Tao, H.; Hwang, S.-W.; Marelli, B.; An, B.; Moreau, J. E.; Yang, M.; Brenckle, M. A.; Kim, S.; Kaplan, D. L.; Rogers, J. A.; Omenetto, F. G. Silk-based resorbable electronic devices for remotely controlled therapy and in vivo infection abatement. *Proc. Natl. Acad. Sci. U. S. A.* **2014**, *111* (49), 17385−17389.

(10) Kundu, B.; Rajkhowa, R.; Kundu, S. C.; Wang, X. Silk fibroin biomaterials for tissue regenerations. *Adv. Drug Delivery Rev.* **2013**, *65* (4), 457−470.

(11) Pritchard, E. M.; Kaplan, D. L. Silk fibroin biomaterials for controlled release drug delivery. *Expert Opin. Drug Delivery* **2011**, *8* (6), 797−811.

(12) Gupta, M. K.; Singamaneni, S.; McConney, M.; Drummy, L. F.; Naik, R. R.; Tsukruk, V. V. A facile fabrication strategy for patterning protein chain conformation in silk materials. *Adv. Mater.* **2010**, *22* (1), 115−119.

(13) Altman, G. H.; Diaz, F.; Jakuba, C.; Calabro, T.; Horan, R. L.; Chen, J.; Lu, H.; Richmond, J.; Kaplan, D. L. Silk-based biomaterials. *Biomaterials* **2003**, *24* (3), 401−416.

(14) Shao, Z.; Vollrath, F. Materials: Surprising strength of silkworm silk. *Nature* **2002**, *418* (6899), 741−741.

(15) Jiang, C.; Wang, X.; Gunawidjaja, R.; Lin, Y. H.; Gupta, M. K.; Kaplan, D. L.; Naik, R. R.; Tsukruk, V. V. Mechanical properties of robust ultrathin silk fibroin films. *Adv. Funct. Mater.* **2007**, *17* (13), 2229−2237.

(16) Shao, Z. Z.; Vollrath, F. Materials: Surprising strength of silkworm silk. *Nature* **2002**, *418* (6899), 741−741.

(17) Gosline, J. M.; Guerette, P. A.; Ortlepp, C. S.; Savage, K. N. The mechanical design of spider silks: From fibroin sequence to mechanical function. *J. Exp. Biol.* **1999**, *202* (23), 3295−3303.

(18) Koh, L.-D.; Cheng, Y.; Teng, C.-P.; Khin, Y.-W.; Loh, X.-J.; Tee, S.-Y.; Low, M.; Ye, E.; Yu, H.-D.; Zhang, Y.-W.; Han, M.-Y. Structures, mechanical properties and applications of silk fibroin materials. *Prog. Polym. Sci.* **2015**, *46*, 86−110.

(19) Chen, X.; Cai, H. F.; Ling, S. J.; Shao, Z. Z.; Huang, Y. F. Conformation transition of Bombyx mori silk protein monitored by time-dependent Fourier transform infrared (FT-IR) spectroscopy: effect of organic solvent. *Appl. Spectrosc.* **2012**, *66* (6), 696−699.

(20) Hu, X.; Shmelev, K.; Sun, L.; Gil, E.-S.; Park, S.-H.; Cebe, P.; Kaplan, D. L. Regulation of silk material structure by temperature-controlled water vapor annealing. *Biomacromolecules* **2011**, *12* (5), 1686−1696.

(21) Dickerson, M. B.; Fillery, S. P.; Koerner, H.; Singh, K. M.; Martinick, K.; Drummy, L. F.; Durstock, M. F.; Vaia, R. A.; Omenetto, F. G.; Kaplan, D. L.; Naik, R. R. Dielectric breakdown strength of regenerated silk fibroin films as a function of protein sonformation. *Biomacromolecules* **2013**, *14* (10), 3509−3514.

(22) Hu, Y. P.; Zhang, Q.; You, R. C.; Wang, L. S.; Li, M. Z. The relationship between secondary structure and biodegradation behavior of silk fibroin scaffolds. *Adv. Mater. Sci. Eng.* **2012**, *2012*, 185905.

(23) Jang, J. H.; Ullal, C. K.; Choi, T. Y.; Lemieux, M. C.; Tsukruk, V. V.; Thomas, E. L. 3D polymer microframes that exploit length-scale-dependent mechanical behavior. *Adv. Mater.* **2006**, *18* (16), 2123−2127.

(24) Shi, Y.; Li, X.; Ding, G.; Wu, Y.; Weng, Y.; Hu, Z. Control of β-sheet crystal orientation and elastic modulus in silk protein by nanoconfinement. *Macromolecules* **2014**, *47* (22), 7987−7992.

(25) Tsioris, K.; Tao, H.; Liu, M. K.; Hopwood, J. A.; Kaplan, D. L.; Averitt, R. D.; Omenetto, F. G. Rapid transfer-based micropatterning and dry etching of silk microstructures. *Adv. Mater.* **2011**, *23* (17), 2015−2019.

(26) Amsden, J. J.; Domachuk, P.; Gopinath, A.; White, R. D.; Negro, L. D.; Kaplan, D. L.; Omenetto, F. G. Rapid nanoimprinting of silk fibroin films for biophotonic applications. *Adv. Mater.* **2010**, *22* (15), 1746−1749.

(27) Brenckle, M. A.; Tao, H.; Kim, S.; Paquette, M.; Kaplan, D. L.; Omenetto, F. G. Protein-protein nanoimprinting of silk fibroin films. *Adv. Mater.* **2013**, *25* (17), 2409−2414.

(28) Perry, H.; Gopinath, A.; Kaplan, D. L.; Dal Negro, L.; Omenetto, F. G. Nano- and micropatterning of optically transparent, mechanically robust, biocompatible silk fibroin films. *Adv. Mater.* **2008**, *20* (16), 3070−3072.

(29) Tao, H.; Kainerstorfer, J. M.; Siebert, S. M.; Pritchard, E. M.; Sassaroli, A.; Panilaitis, B. J. B.; Brenckle, M. A.; Amsden, J. J.; Levitt, J.; Fantini, S.; Kaplan, D. L.; Omenetto, F. G. Implantable, multifunctional, bioresorbable optics. *Proc. Natl. Acad. Sci. U. S. A.* **2012**, *109* (48), 19584−19589.

DOI: 10.1021/acsbiomaterials.6b00177
ACS Biomater. Sci. Eng. XXXX, XXX, XXX−XXX

(30) Kattumenu, R.; Lee, C. H.; Tian, L.; McConney, M. E.; Singamaneni, S. Nanorod decorated nanowires as highly efficient SERS-active hybrids. *J. Mater. Chem.* **2011**, *21* (39), 15218−15223.
(31) Steinhart, M.; Wendorff, J. H.; Greiner, A.; Wehrspohn, R. B.; Nielsch, K.; Schilling, J.; Choi, J.; Gosele, U. Polymer nanotubes by wetting of ordered porous templates. *Science* **2002**, *296* (5575), 1997−1997.
(32) Asakura, T.; Suzuki, Y.; Nakazawa, Y.; Yazawa, K.; Holland, G. P.; Yarger, J. L. Silk structure studied with nuclear magnetic resonance. *Prog. Nucl. Magn. Reson. Spectrosc.* **2013**, *69* (2), 23−68.
(33) Glišović, A.; Salditt, T. Temperature dependent structure of spider silk by X-ray diffraction. *Appl. Phys. A: Mater. Sci. Process.* **2007**, *87* (1), 63−69.
(34) Canetti, M.; Seves, A.; Secundo, F.; Vecchio, G. Cd and small-angle X-ray-scattering of silk fibroin in solution. *Biopolymers* **1989**, *28* (9), 1613−1624.
(35) Rousseau, M. E.; Lefevre, T.; Beaulieu, L.; Asakura, T.; Pezolet, M. Study of protein conformation and orientation in silkworm and spider silk fibers using Raman microspectroscopy. *Biomacromolecules* **2004**, *5* (6), 2247−2257.
(36) Monti, P.; Freddi, G.; Bertoluzza, A.; Kasai, N.; Tsukada, M. Raman spectroscopic studies of silk fibroin from Bombyx mori. *J. Raman Spectrosc.* **1998**, *29* (4), 297−304.
(37) Rousseau, M.-E.; Beaulieu, L.; Lefèvre, T.; Paradis, J.; Asakura, T.; Pézolet, M. Characterization by Raman microspectroscopy of the strain-induced conformational transition in fibroin fibers from the silkworm Samia cynthia ricini. *Biomacromolecules* **2006**, *7* (9), 2512−2521.
(38) Yin, J.; Chen, E.; Porter, D.; Shao, Z. Enhancing the toughness of regenerated silk fibroin film through uniaxial extension. *Biomacromolecules* **2010**, *11* (11), 2890−2895.
(39) Ayutsede, J.; Gandhi, M.; Sukigara, S.; Micklus, M.; Chen, H. E.; Ko, F. Regeneration of Bombyx mori silk by electrospinning. Part 3: characterization of electrospun nonwoven mat. *Polymer* **2005**, *46* (5), 1625−1634.

DOI: 10.1021/acsbiomaterials.6b00177
ACS Biomater. Sci. Eng. XXXX, XXX, XXX−XXX